ChemComm

Accepted Manuscript

This article can be cited before page numbers have been issued, to do this please use: L. Ge, Q. Hong, H. Li and F. Li, *Chem. Commun.*, 2019, DOI: 10.1039/C9CC00889F.

ROYAL SOCIETY OF CHEMISTRY

rsc.li/chemcomm

View Article Online
DOI: 10.1039/C9CC00889F

COMMUNICATION

Laser-induced TiO_2-Decorated Graphene Photoelectrode for Sensitive Photoelectrochemical Biosensing

Received 00th January 20xx,
Accepted 00th January 20xx

DOI: 10.1039/x0xx00000x

Lei Ge,[a] Qing Hong,[a] Hui Li [a] and Feng Li *[a]

Direct-laser-writing of TiO_2-decorated graphene on indium-tin oxide glass was demonstrated to fabricate unique photoelectrode with a rapid and stable photoelectrochemical response under visible light, which was then applied in a photoelectrochemical enzymatic biosensor for sensitive detection of acetylcholinesterase inhibitor.

Since it coupled the well-known merits of both electrochemical and optical methods, photoelectrochemical (PEC) biosensing has drawn more and more attention in recent years and brings many fascinating features.[1] As demonstrated that the important roles of photoelectrode in determining the analytical performance of PEC biosensing, exploring new architecture of photoelectrode towards the improvement of photocurrent conversion efficiency has become a subject of hot research interest. Among various photoelectrode materials, titanium dioxide (TiO_2) is one of the most popular semiconductors in the design of highly efficient photoelectrode with excellent PEC properties because it possesses environmental friendliness, non-toxicity, controllable morphology, inexpensiveness, superior chemical and physical stability, and good biocompatibility.[2-6] To extended the light absorption range and inhibit the electrons-hole recombination rate of TiO_2, hybrid materials made by coupling TiO_2 with graphene have led to the generation of visible light responsive graphene/TiO_2 composites with much improved efficiency of electron–hole pair disassociation and electron collection.[7-12] Unfortunately, the construction of these graphene/TiO_2-based photoelectrode either requires tedious fabrication processes, including the preparation of graphene and synthesis/deposition of photoactive nanomaterials, or needs multiple modification steps on electrode surface. Hence, a facile, robust, and scalable synthetic route towards graphene/TiO_2 based photoelectrode is on demand. Recently, transient CO_2-laser induction on commercially available polyimide sheets has been recognized as a new and appealing direct-writing strategy for large-scale preparation of graphene-based materials under ambient conditions without the requirement of any mask and template.[13] Owing to the high electronic conductivity of laser-induced graphene (LIG) materials from polyimide, remarkable progress has been made towards the fabrication of various LIG-based composite materials.[14] The inherent characters of the embedded nanomaterials have made the LIG a promising platform for high performance electrocatalytic applications.[15] However, despite continuous research efforts in the development of efficient electro-catalysis on LIG materials, no progress has been made to explore the construction of LIG composite materials for photocatalysis or PEC sensing.

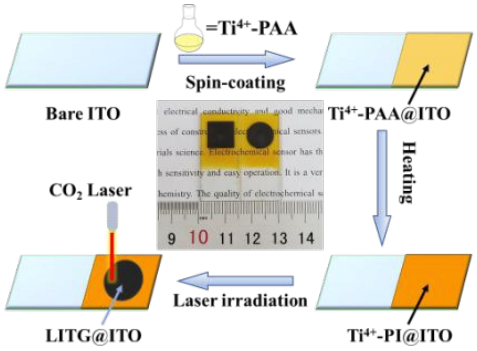

Fig. 1 Schematic illustration for the preparation of LITG@ITO. The inset is photograph of two LITG@ITOs with different geometric size and shape.

Herein, by CO_2 laser induction on a Ti^{4+}-doping polyimide (Ti^{4+}-PI) coated on indium–tin oxide (ITO) glass, we demonstrate a facile and universal approach for direct synthesis of laser-induced TiO_2-decorated graphene (LITG) on the surface of ITO (LITG@ITO) photoelectrode. The detailed procedures for the direct-laser-writing of LITG@ITO are described in ESI and schematically shown in Fig. 1. First, a viscous Ti^{4+}-containing poly(amic acid) (Ti^{4+}-PAA) solution was synthesized and then spin-coated onto the ITO glass substrate. After stepwise heating in a vacuum oven, the PAA layer dehydrates and condenses into polyimide, which was

[a] College of Chemistry and Pharmaceutical Sciences, Qingdao Agricultural University, Qingdao, 266109, People's Republic of China. E-mail: lifeng@qau.edu.cn

Electronic Supplementary Information (ESI) available: [details of any supplementary information available should be included here]. See DOI: 10.1039/x0xx00000x

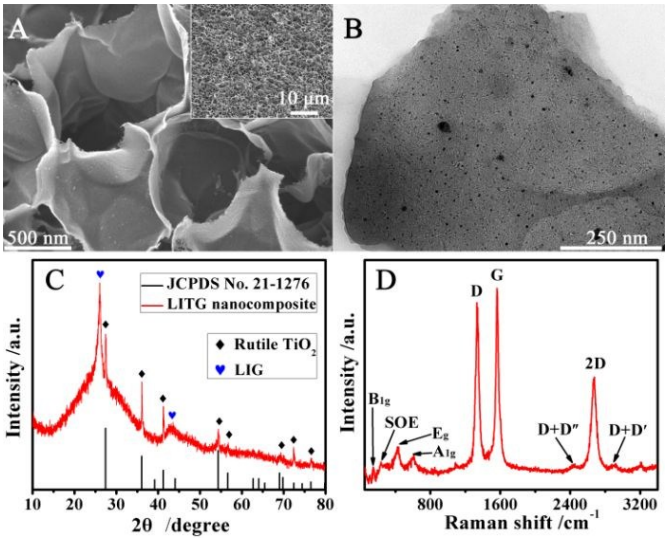

Fig. 2 (A) SEM images of the LITG@ITO. Inset is the corresponding lower magnification SEM image. (B) TEM image, (C) XRD pattern, and (D) Raman spectrum of the LITG nanocomposite.

confirmed by the FTIR measurement (Fig. S2). Then, the obtained Ti^{4+}-PI@ITO was put into a CO_2 laser engraving machine (λ_{laser} =10.6 μm). Under room temperature and ambient air, the laser-irradiated regions of insulating Ti^{4+}-PI on the surface of ITO was photothermally and directly converted into conductive LITG with a sheet resistance of ca. 71.4 Ω/sq. Digital photo of LITG@ITOs are shown in Fig. 1, suggesting that the LITG@ITO can be readily laser-patterned into various geometric size and shape. The morphology of LITG@ITO is shown in Fig. 2A. It is interesting to observe that LITG@ITO derived from Ti^{4+}-PI@ITO shows similar morphology to LIG@ITO derived from PI@ITO in our previous work,[16] without the observation of large TiO_2 nanoparticles, indicating that the doping of titanium(IV) oxyacetylacetonate (Ti^{4+}-OAA) in PI layer has little influence on the formation of 3D interconnected macroporous framework with abundant sharp edges (Fig. 2A). Moreover, the surfaces of the graphene sheets in LITG exhibit a rough morphology (Fig. 2A), implying that there are small TiO_2 nanocrystals attached on the graphene sheets, which was further confirmed by the TEM results in Fig. 2B. As illustrated in Fig. 2B, it is evident that there is a good dispersion of TiO_2 nanocrystals, which have a primary particle size of ca. 3 ~ 12 nm in diameter, on the multi-layered graphene sheet without significant agglomeration. These results were also confirmed by high resolution TEM (Fig. S3), in which the rutile TiO_2 phase planar spacing of the (101) and (111) planes were also clearly observed.

To reach a deeper characterization of the LITG nanocomposite on ITO surface, first, its building components and crystalline phase are elucidated by XRD spectroscopy. As shown in Fig. 2C, an intense and broad diffraction peak centered at ca. 26° (2θ) was observed in the XRD patterns of LITG nanocomposite, corresponding to (002) plane reflection. Another characteristic peak of (100) plane was also identified at ca. 43° (2θ) as a clear indication of the in-plane structure of graphene. These XRD peaks confirm the formation of multilayered graphene sheets in the LITG nanocomposite with a high graphitization degree.[17] Meanwhile, LITG nanocomposite also showed a similar XRD pattern to the typical peaks of rutile (JCPDS card No. 21-1276) at 2θ values of 27.5°, 36°, 41.3°, and 54.3°, which are attributed to the (110), (101), (111), and (211) faces of rutile TiO_2.[18] The tendency of TiO_2 nanocrystals to form rutile phase in LITG nanocomposite, which were also observed in the XRD pattern of laser-induced TiO_2 (LI-TiO_2) on ITO glass (Fig. S4), are mainly attributed to the high localized temperatures under the irradiation of CO_2 laser.[19] It is worth noting that no diffraction pattern from other species have been detected, indicating the high purity and crystallinity of the LITG nanocomposites. The above conclusions can also be further corroborated by the results of Raman spectrum. As shown in Fig. 2D, obviously, the three prominent Raman peaks centered at 1340, 1570, and 2680 cm^{-1} are considered as the characteristic D, G, and 2G band of graphene, respectively.[17] The high D to G ratio as well as the clearly identified D+D" peak and D+D' peak in the Raman spectrum suggest the existence of different defects states,[20] such as the edge defects associated with the sharp edges of graphene sheets observed in SEM image, which is expected not only to improve the electrolyte wettability but also to provide good electric conductivity.[21] Moreover, as the most significant Raman peak of graphene, the intensity and the location of the 2D peak revealed the typical multi-layer characterization of LIG, which is consistent with TEM observation. In addition, the LITG nanocomposite also displays four apparent Raman peaks at 147 cm^{-1} (B_{1g}), 241 cm^{-1} (second-order effect, SOE), 445 cm^{-1} (E_g), and 610 cm^{-1} (A_{1g}),[22] respectively, suggesting the formation of rutile TiO_2 during the laser-scribing of Ti^{4+}-PI@ITO. These observations provide clear evidence for the successful fabrication of LITG@ITO.

Then, the PEC performance of the LITG@ITO was evaluated via the measurements of its time-dependent photocurrent generation using 0.1 M ascorbic acid (AA) as a sacrificial electron donor under the repeat on/off irradiation of visible light (~427 nm LED light source, 100 W/m^2) at a given time interval. As shown in Fig. 3A, following the onset and offset of the irradiation light, the LITG@ITO shows a prompt and stable anodic PEC response (curve a), which could be repeatedly regenerated upon 50 consecutive on/off illumination cycles without significant fluctuations (Fig. S5), demonstrating good operational stability of LITG@ITO for reliable photocurrent collection. Incidentally, the optimal values for the doping amount of Ti^{4+}-OAA was investigated by recording the

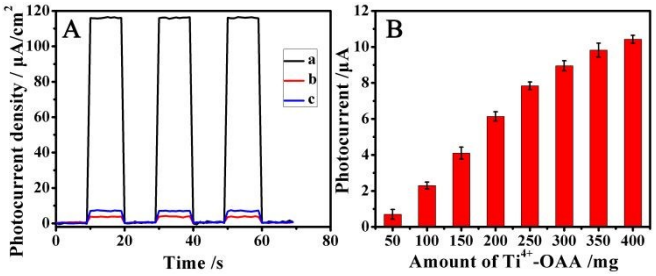

Fig. 3 (A) Photocurrent responses of the laser-induced electrodes, (a) LITG@ITO, (b) LI-TiO_2@ITO, and (c) LIG@ITO. (B) Optimization of the doping amount of Ti^{4+}-OAA in Ti^{4+}-PAA mixture. All error bars in this work represent the standard deviations of 10 parallel tests.

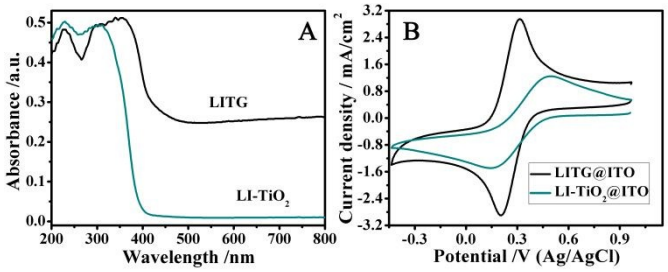

Fig. 4 (A) UV-visible DRS of the LI-TiO_2@ITO and LITG@ITO. (B) CVs of the as-made LI-TiO_2@ITO and LITG@ITO.

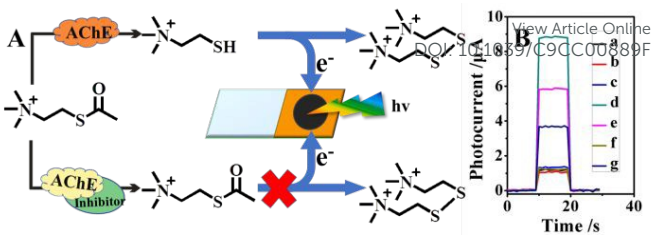

Fig. 5 (A) Principle of the PEC biosensor on LITG@ITO. (B) Photocurrents of LITG@ITO in (a) blank PBS and PBS containing (b) AChE, (c) ATCl, (d) AChE + ATCl, (e) 0.1 ng/mL CP pretreated AChE + ATCl, (f) 0.1 ng/mL CP, and (g) 1.0 ng/mL CP pretreated AChE + ATCl.

photocurrent response and was found to be 400 mg (Fig. 3B). Once the Ti^{4+}-OAA amount exceeds 400 mg, the excessive doping of Ti^{4+}-OAA in PAA would disturb the formation of homogeneous and viscous Ti^{4+}-PAA mixture. Under the optimal conditions, the LITG@ITO outputs a large photocurrent intensity up to ca. 114.4 μA/cm^2 (curve a), which is about 30 times higher than that of the LI-TiO_2@ITO (curve b). In addition, as a control, only a small photocurrent response is obtained from LIG@ITO (curve c), indicating that LIG@ITO by itself cannot act as efficient photoelectrode for generation of photocurrent under visible light. These results revealed that the significantly improved photocurrent generation of LITG@ITO is probably attributed to the altered light absorption feature and facilitated charge transfer after coupling with LIG, similar to the case of graphene/TiO_2 composites obtained via solution-based methods.[7, 10]

To verify the first assumption, the optical properties of these laser-induced photoelectrodes were characterized via UV–visible diffuse reflectance spectra (DRS, Fig. 4A). As expected, a sharp absorption edge was observed at around 400 nm for LI-TiO_2@ITO with almost no absorption in the visible light region, indicating that it cannot be effectively photo-excited by visible light irradiation, which is in agreement to the results in photocurrent measurements. It was clear from Fig. 4A that, compared to LI-TiO_2@ITO, the absorption edge of LITG@ITO undergoes an obvious red shift. Moreover, LITG@ITO shows an enhanced absorbance throughout the visible light region from 400 to 800 nm, which is in line with the black color of the samples (Fig. 1). Furthermore, the plot of the transformed Kubelka-Munk function versus the energy of absorbed light is illustrated in Fig. S6A, from which the roughly estimated band gap values of LITG@ITO and LI-TiO_2@ITO are 2.91 and 3.28 eV, respectively, suggesting a band gap narrowing of the semiconductor TiO_2 in LITG nanocomposites. These results confirm that the coupling of TiO_2 with LIG via the present laser-scribing process can effectively extend the photoresponding range as well as enhance the visible light absorption capability of TiO_2, both of which in turn contribute to the improvement of the PEC performance of LITG@ITO as described above. To shed light on the charge transfer properties of the photoelectrodes, as shown in Fig. 4B, the cyclic voltammograms (CV) of LITG@ITO and LI-TiO_2@ITO were conducted using $[K_3Fe(CN)_6]/[K_4Fe(CN)_6]$ as redox probe at a scan rate of 100 mV/s. It is noticeable that the CV of LITG@ITO presented a larger current density and smaller peak-to-peak separations (ΔE_p) than that of LI-TiO_2@ITO, demonstrating a significantly enhanced charge transfer rate of LITG@ITO. The electrochemical active area of LITG@ITO was calculated to be 24.432 mm^2, which was nearly three times larger than its physical area (9.0 mm^2). Moreover, the interfacial charge transfer properties of the photoelectrodes were also confirmed by electrochemical impedance spectroscopy (EIS, Fig. S6B). Overall, both the improved CV and EIS behavior of LITG@ITO could be ascribed to the presence of the LIG as a highly conducting substrate, which not only provides more accessible active surfaces towards electron donors, but also acts as an efficiently charge acceptor and transporter to shuttle the photogenerated charges from TiO_2, consequently suppressing charge recombination and promoting the efficiency in the photocurrent generation.

The aforementioned experimental results motivated us to explore the potential applicability of LITG@ITO in PEC biosensing. As is well-known, acetylcholinesterase (AChE) plays a significant role in the termination of acetylcholine-mediated neurotransmission. The blocking of AChE by inhibitor continuously stimulates the nerve conduction. Thus, a reliable approach for the sensitive detection of AChE inhibitor is highly desirable. Herein, a PEC platform for AChE inhibitor assay was proposed on LITG@ITO. The PEC biosensing mechanism is represented in Fig. 5A. To evaluate the feasibility of the proposed PEC biosensor for AChE inhibitor, the typical photocurrent responses of this AChE inhibitor assay system were first investigated by using chlorpyrifos (CP) as a proof-of-concept inhibitor. As depicted in Fig. 5B, in comparison with the control experiment in blank electrolyte solution (curve a), either AChE (curve b) or acetylthiocholine (ATCl, curve c) alone caused negligible photocurrent responses. In contrast, the incubation of ATCl with AChE results in a remarkable enhancement of the photocurrent output (curve d). This is attributed to the fact that AChE can catalyze the hydrolysis of ATCl to produce thiocholine as an ideal hole scavenger.[23] Then, an obvious photocurrent decrease was observed when AChE was pretreated with a certain amount of CP (curve e), indicating an impaired enzymatic activity of AChE. In another control experiment, only CP were added into the electrolyte solution in the absence of AChE and ATCl, no obvious photocurrent change was observed (curve f). Moreover, the intensity of photocurrent output decreases as the concentration of AChE inhibitor increased in the solution (curve g), revealing the applicability of the proposed LITG@ITO photoelectrode for subsequent AChE inhibitor assay.

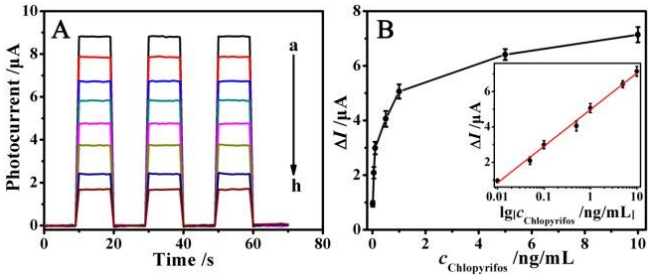

Fig. 6 Photocurrent responses of the PEC biosensor to CP at various concentrations (from a to h: 0, 0.01, 0.05, 0.1, 0.5, 1.0, 5.0, and 10.0 ng/mL. (B) Variation of the photocurrent as a function of c_{CP}. Insert is the linear relationship of ΔI versus the logarithmic value of c_{CP}.

In order to study the sensitivity of the proposed biosensing platform, a series of AChE solutions (5.0 U/mL) inhibited by CP at various concentrations were tested for transient photocurrent responses as described in the ESI under optimal conditions, and the results are shown in Fig. 6A. It was clearly observed that the photocurrent intensity kept decreasing with the increasing of CP concentration (c_{CP}). The change of photocurrent intensity (ΔI) relative to the background (c_{CP} = 0 ng/mL) was employed as the quantitative signal. The derived calibration curve in Fig. 6B demonstrated that ΔI was linearly dependent on the logarithm values of CP concentrations ranging from 0.01 ng/mL to 10 ng/mL. The linear relationship between ΔI and c_{CP} could be described as ΔI (μA) = 4.971 + 2.068lg[c_{CP} (ng/mL)] with a correlation coefficient r = 0.9957). The limit of detection was calculated to be 5.4 pg/mL (c.a. 15.4 pM) at the signal-to-noise ratio of 3σ, which is superior or comparable to the well-developed biosensor for AChE inhibitor (CP) in previous reports as summarized in Table S1. In addition, each data point in the calibration curve represents ten repetitive and parallel measurements of CP using independent LITG@ITO photoelectrodes, which show the relative standard deviations (n=10) ranging from 3.12% to 10.52%, indicating an acceptable reproducibility. Moreover, the proposed PEC sensor also showed a good selectivity toward AChE inhibitor (Fig. S7A) with high operational and storage stability (Fig. S7B,C). These results suggest that the proposed LITG@ITO photoelectrode would be a promising PEC platform for immobilization-free biosensing.

Conclusions

In summary, a visible-light-active photoelectrode was prepared through the in-situ generation of LITG nanocomposite on ITO glass by a facile and scalable direct-laser-writing approach in ambient air at room temperature. This work not only provided a promising paradigm for the direct-laser-writing of unconventional photoelectrode that can be used for sensitive PEC biosensing purposes, but also paves a new way towards the convenient preparation of free-standing photoelectrode for a broad range of applications.

This work was financially supported by National Natural Science Foundation of China (31501570 and 21575074), Basic Research Program of Qingdao (16-5-1-55-jch), Research Foundation for Distinguished Scholars of Qingdao Agricultural University (663-1115003), and the Special Foundation for Distinguished Taishan Scholar of Shandong Province (ts201511052).

Conflicts of interest

There are no conflicts to declare.

Notes and references

1 W.-W. Zhao, J.-J. Xu and H.-Y. Chen, *Chem. Rev.*, 2014, **114**, 7421-7441.
2 J. Shu, Z. Qiu, S. Lv, K. Zhang and D. Tang, *Anal. Chem.*, 2018, **90**, 2425-2429.
3 Z. Song, G.-C. Fan, Z. Li, F. Gao and X. Luo, *Anal. Chem.*, 2018, **90**, 10681-10687.
4 H. Li, J. Li, Y. Zhu, W. Xie, R. Shao, X. Yao, A. Gao and Y. Yin, *Anal. Chem.*, 2018, **90**, 5496-5502.
5 X. Li, L. Zhu, Y. Zhou, H. Yin and S. Ai, *Anal. Chem.*, 2017, **89**, 2369-2376.
6 L.-M. Yu, Y.-C. Zhu, Y.-L. Liu, P. Qu, M.-T. Xu, Q. Shen and W.-W. Zhao, *Anal. Chem.*, 2018, **90**, 10803-10811.
7 W. Ma, D. Han, S. Gan, N. Zhang, S. Liu, T. Wu, Q. Zhang, X. Dong and L. Niu, *Chem. Commun.*, 2013, **49**, 7842-7844.
8 L. Wang, W. Ma, S. Gan, D. Han, Q. Zhang and L. Niu, *Anal. Chem.*, 2014, **86**, 10171-10178.
9 M. Nallal, G. Anantha Iyengar and K. Pill-Lee, *ACS Appl. Mater. Interfaces*, 2017, **9**, 37166-37183.
10 H. Zhang, X. Lv, Y. Li, Y. Wang and J. Li, *ACS Nano*, 2010, **4**, 380-386.
11 N. Hao, R. Hua, S. Chen, Y. Zhang, Z. Zhou, J. Qian, Q. Liu and K. Wang, *Biosens. Bioelectron.*, 2018, **101**, 14-20.
12 X.-M. Shi, C.-D. Wang, Y.-C. Zhu, W.-W. Zhao, X.-D. Yu, J.-J. Xu and H.-Y. Chen, *Anal. Chem.*, 2018, **90**, 9687-9690.
13 R. Ye, D. K. James and J. M. Tour, *Acc. Chem. Res.*, 2018, **51**, 1609-1620.
14 R. Ye, Z. Peng, T. Wang, Y. Xu, J. Zhang, Y. Li, L. G. Nilewski, J. Lin and J. M. Tour, *ACS Nano*, 2015, **9**, 9244-9251.
15 J. Zhang, C. Zhang, J. Sha, H. Fei, Y. Li and J. M. Tour, *ACS Appl. Mater. Interfaces*, 2017, **9**, 26840-26847.
16 Q. Hong, L. Yang, L. Ge, Z. Liu and F. Li, *Analyst*, 2018, **143**, 3327-3334.
17 J. Lin, Z. Peng, Y. Liu, F. Ruiz-Zepeda, R. Ye, E. L. G. Samuel, M. J. Yacaman, B. I. Yakobson and J. M. Tour, *Nat. Commun.*, 2014, **5**, 5714.
18 X. Pan, Y. Zhao, S. Liu, C. L. Korzeniewski, S. Wang and Z. Fan, *ACS Appl. Mater. Interfaces*, 2012, **4**, 3944-3950.
19 J. Li, Z. Wang, J. Wang and T.-K. Sham, *J. Phys. Chem. C*, 2016, **120**, 22079-22087.
20 A. C. Ferrari and D. M. Basko, *Nat. Nanotechnol.*, 2013, **8**, 235.
21 D. A. C. Brownson, D. K. Kampouris and C. E. Banks, *Chem. Soc. Rev.*, 2012, **41**, 6944-6976.
22 Y. Zhang, C. X. Harris, P. Wallenmeyer, J. Murowchick and X. Chen, *J. Phys. Chem. C*, 2013, **117**, 24015-24022.
23 W.-W. Zhao, S. Shan, Z.-Y. Ma, L.-N. Wan, J.-J. Xu and H.-Y. Chen, *Anal. Chem.*, 2013, **85**, 11686–11690.